Molecular Therapy
Nucleic Acids
Original Article

DNA/RNA heteroduplex technology with cationic oligopeptide reduces class-related adverse effects of nucleic acid drugs

Masahiro Ohara,[1,2,3] Tetsuya Nagata,[1,2,3] Rintaro Iwata Hara,[1,2,3] Kie Yoshida-Tanaka,[1,2] Nozomi Toide,[1,2] Kazunori Takagi,[4] Kazuki Sato,[4] Tomoya Takenaka,[5] Masanori Nakakariya,[5] Kenichi Miyata,[5] Yusuke Maeda,[4] Kazuko Toh,[1,2,3] Takeshi Wada,[4] and Takanori Yokota[1,2,3]

[1]Department of Neurology and Neurological Science, Graduate School of Medical and Dental Science, Tokyo Medical and Dental University, Tokyo 113-8519, Japan; [2]NucleoTIDE and PepTIDE Drug Discovery Center, Tokyo Medical and Dental University, Tokyo 113-8519, Japan; [3]Center for Brain Integration Research, Tokyo Medical and Dental University, Tokyo 113-8519, Japan; [4]Faculty of Pharmaceutical Sciences, Tokyo University of Science, Chiba 278-8510, Japan; [5]Takeda Pharmaceutical Company Limited, Kanagawa 251-8555, Japan

Antisense oligonucleotides (ASOs) are a therapeutic modality for incurable diseases. However, systemic injection of gapmer-type ASOs causes class-related toxicities, including prolongation of activated partial thromboplastin time (aPTT) and thrombocytopenia. We previously reported that cholesterol-conjugated DNA/RNA heteroduplex oligonucleotides (Chol-HDOs) exhibit significantly enhanced gene-silencing effects compared to ASOs, even in the central nervous system, by crossing the blood-brain barrier. In the present study, we initially evaluated the effect of the HDO structure on class-related toxicities. The HDO structure ameliorated the class-related toxicities associated with ASOs, but they remained to some extent. As a further antidote, we have developed artificial cationic oligopeptides, L-2,4-diaminobutanoic acid oligomers (DabOs), which bind to the phosphates in the major groove of the A-type double-helical structure of HDOs. The DabO/Chol-HDO complex showed significantly improved aPTT prolongation and thrombocytopenia in mice while maintaining gene-silencing efficacy. Moreover, the conjugation with DabOs effectively prevented cerebral infarction, a condition frequently observed in mice intravenously injected with high-dose Chol-HDO. These approaches, combining HDO technology with DabOs, offer distinct advantages over conventional strategies in reducing toxicities. Consequently, the DabO/HDO complex represents a promising platform for overcoming the class-related toxicities associated with therapeutic ASOs.

INTRODUCTION

Antisense oligonucleotides (ASOs) represent a therapeutic platform for incurable diseases, including neurodegenerative diseases. Although several ASOs have been marketed so far, systemic administration of high-dose ASOs can cause various side effects.[1–4] The potential adverse effects of gapmer-type ASOs are classified into two categories: hybridization-dependent toxicities due to on- or off-target effects and hybridization-independent toxicities due to non-antisense effects of ASOs including non-specific binding to various proteins and proinflammatory activity.[5] ASO hybridization-dependent toxicities are caused by the binding of ASOs to RNA with similar sequences to that of the target RNA. On the contrary, ASO hybridization-independent toxicities are sequence independent and class related, accounting for most of the observed toxicities. These class-related toxicities, such as thrombocytopenia and activated partial thromboplastin time (aPTT) prolongation, are demonstrated in a drug-concentration-dependent manner[1,4] and thus lead to safety concerns about high-dose systemic administration of ASOs.

We have developed lipid-conjugated heteroduplex oligonucleotides (HDOs), which produce much higher gene-silencing effects of target RNA than ASOs by systemic administration.[6,7] HDOs consist of the DNA strand and the complementary RNA strand (cRNA), and the center gap portion of DNA/RNA is recognized and cleaved by endogenous RNase H, making the parent ASO released to be active. In addition, HDOs can conjugate various ligands at the cRNA strand without affecting the efficacy of ASO strands. The high effectiveness of cholesterol-conjugated HDOs (Chol-HDOs) can be attributed to its

Received 30 May 2023; accepted 26 July 2024;
https://doi.org/10.1016/j.omtn.2024.102289.

Correspondence: Tetsuya Nagata, MD, PhD, Department of Neurology and Neurological Science, Graduate School of Medical and Dental Sciences, Tokyo Medical and Dental University, 1-5-45 Yushima, Bunkyo-ku, Tokyo 113-8519, Japan.
E-mail: t-naga.nuro@tmd.ac.jp
Correspondence: Rintaro Iwata Hara, PhD, Department of Neurology and Neurological Science, Graduate School of Medical and Dental Sciences, Tokyo Medical and Dental University, 1-5-45 Yushima, Bunkyo-ku, Tokyo 113-8519, Japan.
E-mail: haranuro@tmd.ac.jp
Correspondence: Takanori Yokota, MD, PhD, Department of Neurology and Neurological Science, Graduate School of Medical and Dental Sciences, Tokyo Medical and Dental University, 1-5-45 Yushima, Bunkyo-ku, Tokyo 113-8519, Japan.
E-mail: tak-yokota.nuro@tmd.ac.jp

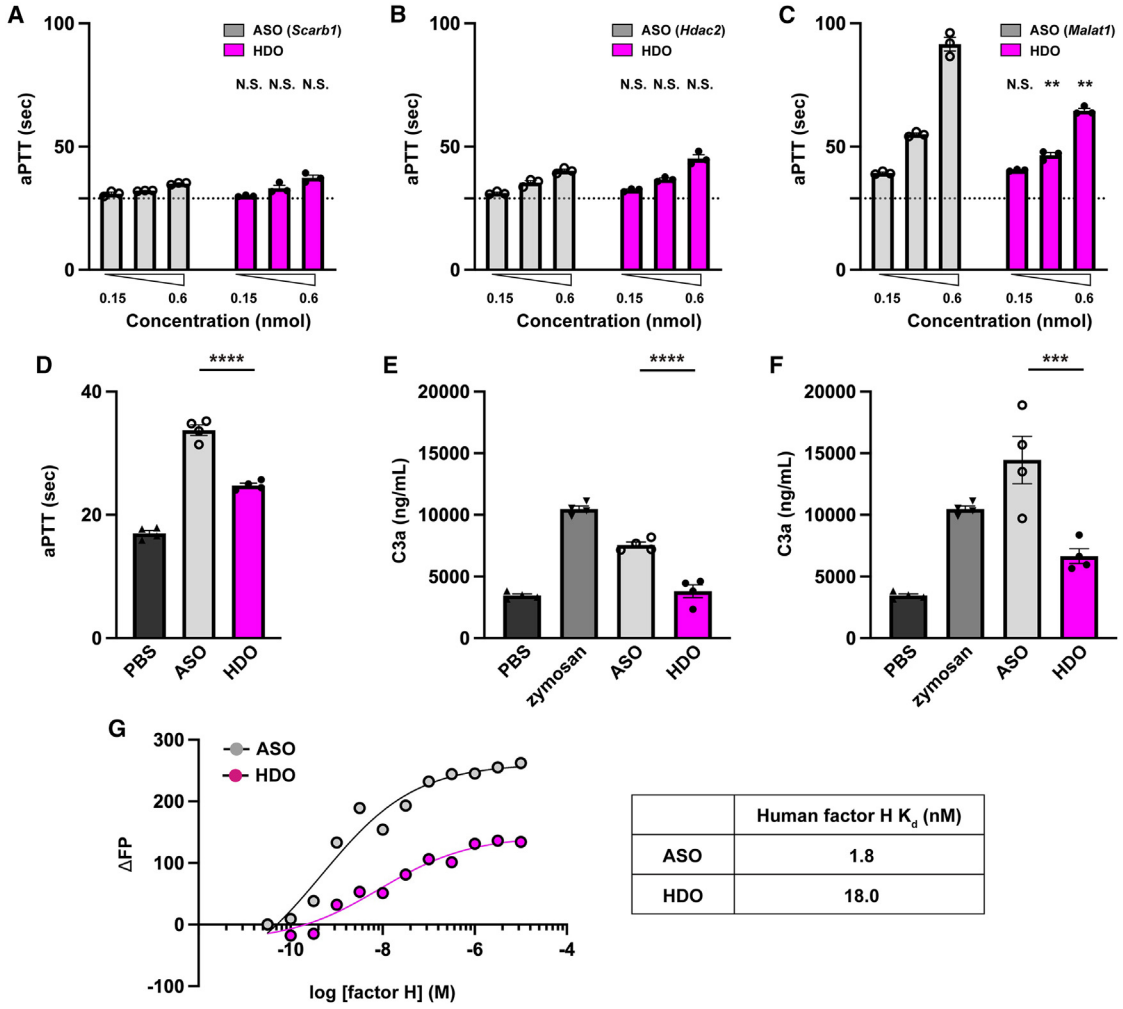

Figure 1. Effects of ASO and HDO on activated partial thromboplastin times

(A–C) Effects on activated partial thromboplastin time (aPTT) of 14-mer ASO and HDO targeting *Scarb1* mRNA (A), 16-mer ASO and HDO targeting *Hdac2* mRNA (B), and 16-mer ASO and HDO targeting *Malat1* RNA (C). The dotted line represents aPTT of human plasma without adding any ASO or HDO. (D) aPTT in mice intravenously injected with 16-mer ASO and HDO targeting *Malat1* RNA (20 mg/kg as the parent ASO). (E and F) Effects on complement activation of 16-mer ASO and HDO targeting *Malat1* RNA (E) and 20-mer ASO and HDO targeting *Malat1* RNA (F). (G) Binding curves of 16-mer ASO and HDO to human factor H. Data are presented as mean ± SEM, $n = 3$ per group; N.S., not significant; $^{*}p < 0.05$, $^{**}p < 0.01$, $^{***}p < 0.001$, $^{****}p < 0.0001$ compared to ASO. In (A)–(C), aPTTs in ASO and HDO with the same concentrations are statistically compared. In (D)–(F), only the statistical comparison between ASO and HDO among the multiple comparisons is described.

increased blood retention *in vivo*, leading to higher drug concentrations in the tissues and more effective cellular uptake than ASOs.[6–8] Intriguingly, Chol-HDOs achieve effective gene knockdown in the central nervous system (CNS) by crossing the blood-brain barrier (BBB), and genes even in deep brain regions can be effectively inhibited by systemic injection.[7] There have been some challenges regarding oligonucleotide therapeutics targeting neurodegenerative diseases. For example, one approved antisense drug, nusinersen, and other drug candidates for various neurodegenerative diseases require intrathecal administration,[9–12] subjecting patients to lifelong invasive procedures. Furthermore, despite the direct intrathecal administration of ASOs into the CNS, they are poorly distributed to deep brain regions.[13,14] The HDO technology can overcome these limitations of ASOs and hence is a promising therapeutic modality for neurodegenerative diseases. However, gene inhibition in the CNS requires high-dose intravenous administration of Chol-HDOs, which sometimes causes severe side effects, including focal brain necrosis.[7]

L-2,4-Diaminobutanoic acid (Dab) oligomers (DabOs) were developed as artificial cationic peptides binding to the major groove of RNA/RNA duplexes.[15] Various cationic amino acid oligomers were synthesized, and Dab, which has an aminoethyl side chain, was the most suitable for increasing the stability of the RNA/RNA duplex.[15] Their mixture spontaneously formed the complex of DabOs and

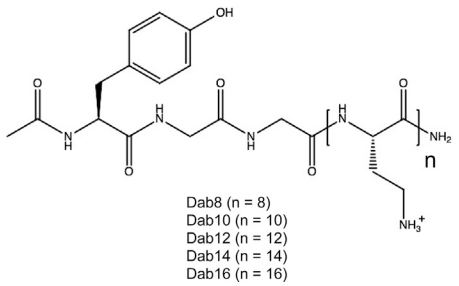

Figure 2. Structures of Dab oligomers used in this study

RNA/RNA duplexes, and DabOs also increased the nuclease resistance of small interfering RNA without disturbing RNAi activity.[16] DNA/RNA duplex forms an A-type double-helical structure as well,[17] and thus DabOs are expected to bind to DNA/RNA duplex.[18] Indeed, DabOs can enhance RNase A resistance of DNA/RNA duplex, but interestingly they also increase RNase H activity.[18] Remarkably, the binding affinity of DabOs to the A-type double-helical structure far exceeds that of just an electrostatic interaction. Consequently, in the complex of DabOs and RNA/RNA or DNA/RNA duplexes, the N/P ratio, i.e., the stoichiometric ratio of the number of cationic groups (N, typically amino and guanidino groups) to that of anionic groups (P, typically phosphodiester and phosphorothioate groups in oligonucleotides), is much lower than that of the previously reported cationic molecules.[19–21] Given that many cations potentially result in toxicity,[22] DabOs have an advantage of safety in developing therapeutic oligonucleotide drugs.

In this study, we initially evaluated the ASO class-related toxicities in HDOs. Moreover, we studied the pharmacological profiles of the DabO/Chol-HDO complex, which is a markedly distinct approach compared to the conventional strategy employed for enhancing the therapeutic potential of oligonucleotide drugs such as backbone or sugar modifications.

RESULTS

The effect of HDO formation on class-related toxicities

We initially evaluated the class-related toxicities of ASOs in HDOs. Effects of ASOs and HDOs with the same sequence on aPTT and complement activation were investigated (Figure 1). In *ex vivo* assay, phosphorothioate (PS)-ASO demonstrated dose-dependent aPTT prolongation as previously reported,[1,2,23] and HDO also demonstrated dose-dependent aPTT prolongation. The aPTT prolongation caused by ASOs is in a PS-related manner,[24,25] and HDOs contain PS modifications in both ASO and cRNA strands (Table S1). However, intriguingly, HDOs demonstrated a similar or shorter aPTT compared to ASOs with the same concentration despite having an increased number of PS modifications (Figures 1A–1C). In the *in vivo* experiment, although the HDO technology improved prolonged aPTT after intravenous ASO injection (20 mg/kg as the parent ASO), it remained to some extent (Figure 1D). Moreover, we assessed the effect of HDO formation on complement activation as another class-related toxicity. We measured C3a levels by ELISA using ASOs and HDOs in different base lengths. HDOs significantly decreased C3a levels compared to ASOs in both base lengths in the *ex vivo* assay (Figures 1E and 1F). To address the mechanisms of reducing toxicities, we evaluated the binding affinities of ASOs and HDOs with human factor H, which is associated with complement activation.[26] A fluorescence polarization assay showed that HDOs have approximately 10-fold reduced binding affinity with human factor H compared to ASOs (Figure 1G).

Dab oligomers bind to HDO or ligand-conjugated HDO but not to ASO

We previously showed that DabOs (Figure 2) bind to natural DNA/RNA duplex and increase the thermal stability more than other cationic oligopeptides, including the octamer of L-lysine.[18] Also, we confirmed that DabO increases T_m values of Chol-HDO more than the octamer of L-lysine (Figures S1A and S1B). Here, we evaluated the binding of DabOs to ligand-conjugated HDOs with gapmer-type ASOs with locked nucleic acid at the wing by electrophoresis (Figure 3). 16-mer Chol-HDO targeting for metastasis-associated lung adenocarcinoma transcript 1 (*Malat1*) RNA and 20-mer Chol-HDO targeting for superoxide dismutase 1 (*SOD1*) mRNA were designed, and their bindings with DabOs (Dab8, Dab12, and Dab16) were evaluated (Figure 3A and Table S1). Their parent ASO sequences were identical to those in previous reports.[7,27] We first confirmed the binding specificity of DabOs to Chol-HDOs compared to ASOs using Alexa 647-labeled 16-mer ASO and Chol-HDO targeting for mouse *Malat1* RNA and 5′ fluorescein (FAM)-labeled Dab12 (Figure 3B). Most of the ASO did not change electrophoretic mobility despite adding Dab12, and most Dab12 were stacked in the well. In contrast, the mixture of Dab12 and Chol-HDO showed merged bands, and the bands corresponding to Chol-HDO disappeared as the amount of DabO increased. These results suggest that DabOs do not strongly bind to ASOs but specifically to Chol-HDOs. We also compared the binding property of Chol-HDO with Dab12 to that of Chol-HDO with the dodecamer of L-lysine (Lys12) (Figures S1C–S1E). The K_D (dissociation constant) value between Dab12 and Chol-HDO was lower than that between Lys12 and Chol-HDO, suggesting the superiority of DabOs in the binding affinity to Chol-HDO. In the following, the mixing molar ratio was defined as the molar ratio of DabOs to Chol-HDOs in the DabO/Chol-HDO complex.

We then evaluated the complex formation of DabOs with different lengths and non-fluorescence-labeled ligand-conjugated HDOs with different base lengths by electrophoresis. In this assay, 20–60 pmol of DabOs were added to 20 pmol of Chol-HDO to form DabO/Chol-HDO complex with different mixing molar ratios (1:1–3:1). For 16-mer Chol-HDO, the upper band representing the complex formation with DabO was weaker in Dab8/Chol-HDO than in Dab12/Chol-HDO complex by a visual assessment (Figure 3C). To quantitatively evaluate the binding affinity, the fraction of DabO/Chol-HDO complex was determined using the equation: bound/(bound + unbound). The fraction of the complex was then plotted

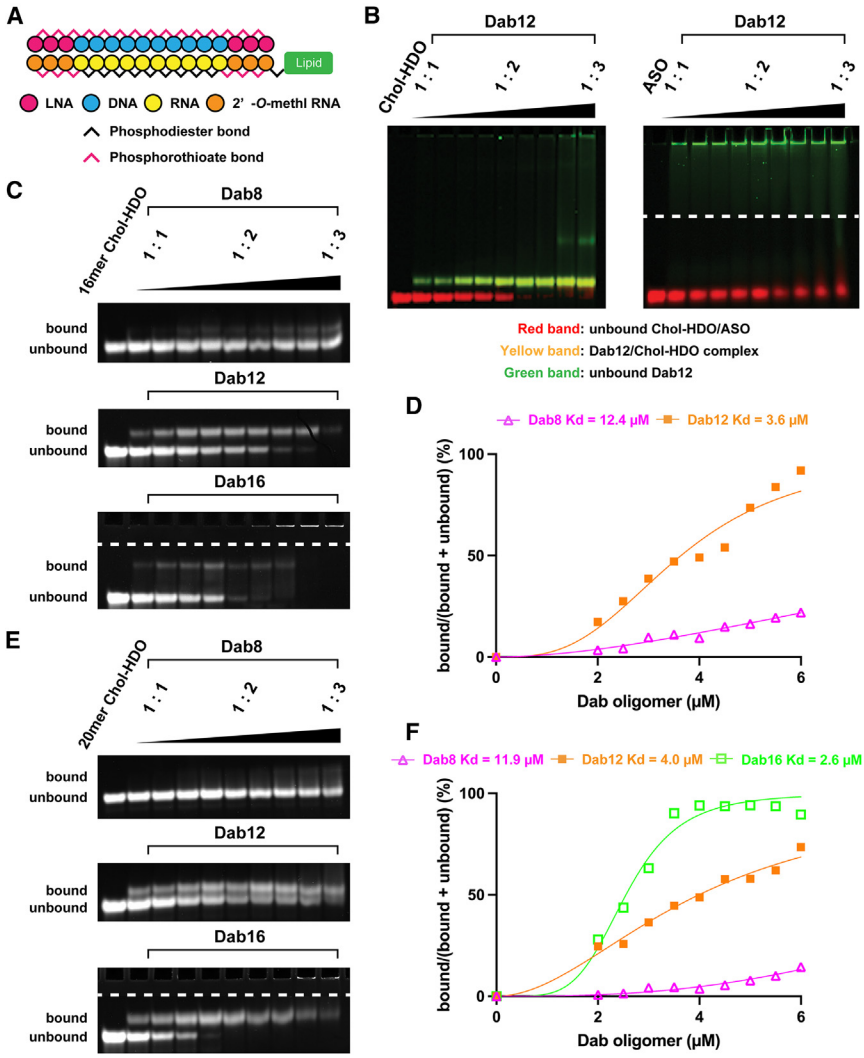

Figure 3. Electrophoresis of ligand-conjugated HDO and Dab oligomer/ligand-conjugated HDO complex

(A) Structures of the ligand-conjugated HDOs. The desired lipid is conjugated to the 5′ end of the cRNA strand of the HDO. (B) Electrophoresis of 20 pmol of FAM-labeled Dab12/Alexa 647-labeled Chol-HDO (left panel) and 20 pmol of FAM-labeled Dab12/Alexa 647-labeled ASO mixture (right panel) in a non-denaturing acrylamide gel. The mixture of Dab12 and Chol-HDO showed a merged band (yellow bands), while ASO (red bands) and Dab12 (green bands) did not show a merged band. (C) Electrophoresis of DabOs/16-mer Chol-HDO complex targeting *Malat1* RNA in non-denaturing acrylamide gel with post-staining. DabOs were added to 20 pmol of Chol-HDO and incubated for 30 min at room temperature to form a complex. For Dab16/Chol-HDO complex, the image for the wells is also shown above the dotted line. (D) Binding curves of Dab8 and Dab12 to 16-mer Chol-HDO. (E) Electrophoresis of DabOs/20-mer Chol-HDO complex targeting *SOD1* mRNA in non-denaturing acrylamide gel with post-staining. DabOs were added to 20 pmol of Chol-HDO and incubated for 30 min at room temperature to form a complex. For Dab16/Chol-HDO complex, the image for the wells is also shown above the dotted line. (F) Binding curves of Dab8, Dab12, and Dab16 to 20-mer Chol-HDO.

versus the concentration of DabO, and K_D values were calculated (Figure 3D).[28] This analysis demonstrated a stronger binding affinity of Dab12 than Dab8 to Chol-HDO. On the contrary, the complex of 16-mer Chol-HDO with excessive Dab16 relative to Chol-HDO was not electrophoresed (Figure 3C). Based on these results, Dab12 seemed a more optimal peptide length than Dab8 and Dab16 for 16-mer Chol-HDO in terms of the binding affinity. For 20-mer Chol-HDO, the lower band representing non-combined Chol-HDO disappeared in lanes where the Dab16/Chol-HDO complex at a mixing molar ratio of more than 1.75:1 was applied (Figure 3E). Conversely, the lower band representing non-combined Chol-HDO did not disappear even in lanes where the Dab8 or Dab12/Chol-HDO complex at a mixing molar ratio of 3:1 was applied by a visual assessment (Figure 3E). A quantitative analysis of the gel also indicated the stronger binding affinity of Dab16 compared to Dab8 and Dab12 (Figure 3F). These results indicated that Dab16 seemed to be a more optimal peptide length than Dab12 for 20-mer Chol-HDO in terms of the binding affinity. Taken together, Chol-HDO with different nucleotide lengths may have an optimal length of DabOs and an optimal molar ratio to DabOs.

Competitive binding assay of Dab oligomers with different lengths to Chol-HDOs by FRET technique

We also confirmed the binding property of DabOs by using the fluorescence resonance energy transfer (FRET) technique (Figure S2). Alexa 568-labeled Chol-HDO and FAM-labeled Dab12 were used in this experiment. Before the experiments, we confirmed the energy transfer using these fluorescent groups in PBS (Figure S2A). Next, we evaluated the relative strength of DabOs binding to 16-mer Chol-HDO. First, Alexa 568-labeled 16-mer Chol-HDO and non-fluorescence-labeled Dab8 or Dab12 were incubated, and FAM-labeled Dab12 was then added. FRET signal was analyzed at 20 min after adding FAM-labeled Dab12 by an i-control instrument (Tecan, Männedorf, Switzerland).[21] A high FRET signal will be observed if the added FAM-labeled Dab12 replaces the pre-binding non-labeled DabOs (Figure S2B). FRET signal was smaller in the Dab12 pre-incubated groups than in Dab8 pre-incubated groups, suggesting that binding strength of Dab12 to Chol-HDO was greater than that of Dab8 (Figure S2C). The FRET signal in an equimolar amount of Dab8 pre-incubated group was the same as that in the control group, which can be explained by the binding capacity of the major groove (Figure S2D). The major groove of 16-mer HDO consists of about 16 phosphate or phosphorothioate groups. Therefore, a mole of Dab8 cannot occupy the major groove, and FAM-Dab12 can bind

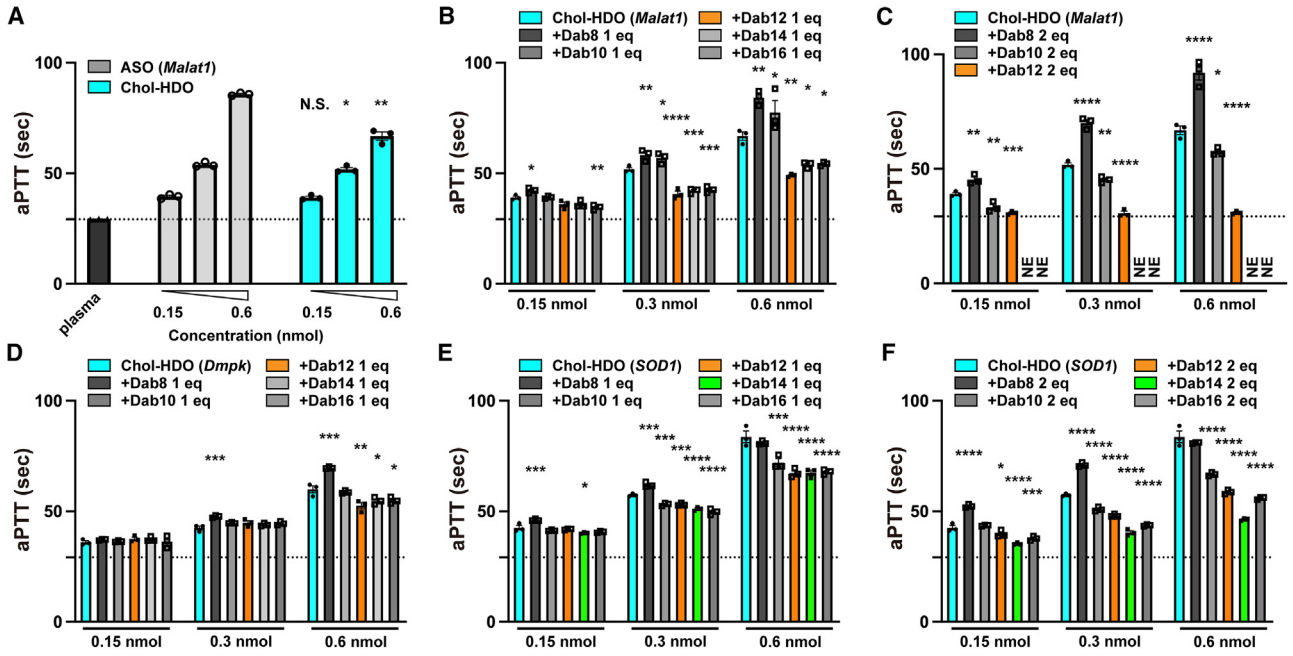

Figure 4. *Ex vivo* or *in vivo* effects of Chol-HDO and Dab oligomer/Chol-HDO complex on activated partial thromboplastin times

(A) Effects of ASO and Chol-HDO in different concentrations on aPTT in normal human plasma. The dotted line represents aPTT of human plasma without adding any ASO, Chol-HDO, or DabO/Chol-HDO complex. (B–F) Effects of DabOs/Chol-HDO complex on aPTT. (B and C) DabOs/16-mer Chol-HDO complex targeting *Malat1* RNA. (B) aPTT was significantly shorter in Dab12, 14, or 16/Chol-HDO complex at the mixing molar ratio of 1:1 than in Chol-HDO only. (C) aPTT was significantly shorter in Dab10 or 12/Chol-HDO complex (2:1) than in Chol-HDO only, while turbidity was observed in Dab14 or 16/Chol-HDO complex solution. (D) DabOs/16-mer Chol-HDO complex targeting *Dmpk* mRNA. aPTT was significantly shorter in Dab12, 14, or 16/Chol-HDO complex (1:1) than in Chol-HDO. (E and F) DabOs/20-mer Chol-HDO complex targeting human *SOD1* mRNA. aPTT was significantly shorter in Dab10, 12, 14, or 16/Chol-HDO complex (1:1 or 2:1) than in Chol-HDO. Dab14/Chol-HDO complex (2:1) showed the shortest aPTT. Results are expressed as mean ± SEM; $n = 3$ per group; $^{*}p < 0.05$, $^{**}p < 0.01$, $^{***}p < 0.001$, $^{****}p < 0.0001$ compared to Chol-HDO with the same concentrations. NE, not examined due to aggregates identified by visual observation. Dab X eq represents the X molar equivalents of Dab oligomers to Chol-HDO.

to the major groove together with non-labeled Dab8 (Figure S2D, upper panel), while two moles of Dab8 can occupy the major groove (Figure S2D, lower panel). In Dab12 pre-incubated groups, the FRET signal became smaller as the mixing molar ratio of unlabeled Dab12 increased from 1:1 to 3:1 (Figure S2C). These results indicate that length/dose dependencies of the binding potential of DabOs were consistent with the aforementioned results of electrophoresis.

Dab oligomer/Chol-HDO complex ameliorates prolonged aPTT *ex vivo*

To investigate the mitigating effect of DabOs on class-related toxicities, we focused on the prolongation of aPTT caused by PS-ASOs.[1,2,23] We evaluated the effect of the DabOs/Chol-HDO complex on aPTT (Figure 4). ASO and Chol-HDO targeting mouse *Malat1* RNA showed dose-dependent aPTT prolongation (Figure 4A). Intriguingly, the complex of 16-mer Chol-HDO and Dab12, Dab14, or Dab16 at the mixing molar ratio of 1:1 suppressed aPTT prolongation compared to Chol-HDO only at 0.3 and 0.6 nmol, while the complex of Chol-HDO and Dab8 or Dab10 rather worsened aPTT (Figure 4B). Among DabOs, Dab12/Chol-HDO complex (1:1 and 2:1) showed the shortest aPTT (Figures 4B and 4C). This ameliorating effect of DabOs on aPTT prolongation was confirmed in another 16-mer sequence targeting mouse *Dmpk* mRNA (Figure 4D). As for 20-mer Chol-HDO, aPTT was significantly shorter in Dab10, 12, 14, or 16/Chol-HDO complex (1:1 and 2:1) than in Chol-HDO only (Figures 4E and 4F). Dab14/Chol-HDO complex (2:1) showed the shortest aPTT. These results showed that the optimal length of DabOs for different lengths of Chol-HDO to suppress aPTT prolongation might exist; Dab12 seemed an optimal oligomer length for 16-mer Chol-HDO (Figures 4B–4D), while Dab14 seemed optimal for 20-mer Chol-HDO (Figure 4F).

Site-specific effects of PS modifications in HDO in aPTT

Next, we evaluated the impact of the position of PS modifications in HDOs on aPTT prolongation. We designed 20-mer ASOs and cRNAs targeting *Malat1* RNA with different PS modification patterns (Figure S3A), and their effects on aPTT were evaluated. For the typical HDO structure with a fully PS-modified ASO as the parent strand, the cRNA strand with PS modifications only in its wing portion demonstrated the most potent suppression of aPTT (Figures S3B and S3C). Moreover, some trends combining 3′-rich PS modifications in ASOs and 3′-rich PS modifications in cRNAs led to more prolonged aPTT. In contrast, ASOs with full or 5′-rich PS modifications resulted in more reduced aPTT upon HDO formation (Figures S3B

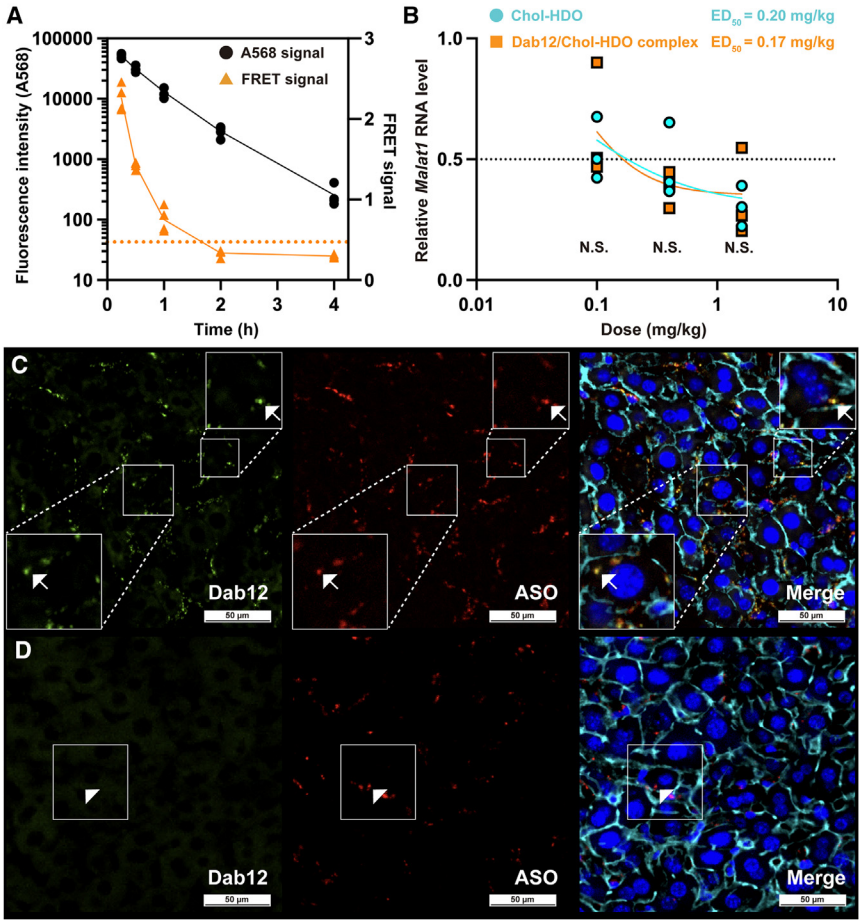

Figure 5. Pharmacokinetics, pharmacodynamics, and histopathological study after administration of low-dose Chol-HDO or Dab oligomer/Chol-HDO complex

(A) Time-dependent changes of Alexa 568 signal and the FRET signal in the mouse serum treated with FAM-labeled Dab12/Alexa 568-labeled Chol-HDO complex (1 mg/kg as the parent ASO) at the mixing molar ratio of 1:1. Dotted line represents the FRET signal of serum from PBS-injected mice. (B) Dose-response relationship of gene inhibition after Chol-HDO or Dab oligomer/Chol-HDO in the liver. *Malat1* RNA expression levels were measured by RT-qPCR. ED_{50} was calculated as the amounts of the parent ASOs. ANOVA with post hoc Tukey's test was performed at the same concentrations. (C and D) Confocal laser scanning microscopy images of mouse livers at 0.5 h (C) or 3 h (D) after injection of FAM-labeled Dab12/Alexa 647-labeled Chol-HDO complex (1 mg/kg as the parent ASO) targeting mouse *Malat1* RNA. The fluorescence signal of Dab12 (green) and that of the parent ASO (red) colocalized in the hepatocytes (arrows) as well as the non-parenchymal cells at 0.5 h after injection (C). On the contrary, the signal of Dab12 was not observed at 3 h after injection. In contrast, the parent ASO fluorescence signal was observed in the hepatocytes and the non-parenchymal cells (arrowheads) (D). Data are presented as the mean; n = 3 or 4 per group; N.S., not significant. Scale bars, 50 μm.

and S3C). The position of PS modifications in HDOs could explain these trends. As a double-stranded structure, HDO contains some phosphates around the 5′ terminus within the major groove of the double strand. PS modifications located in the major groove interact less with proteins, as they are hidden in the groove and thus are less involved in aPTT prolongation. On the contrary, PS modifications around the 3′ terminus of ASO or cRNA face outside and can freely interact with various proteins, resulting in more prolonged aPTT. However, aPTT prolongation remained in all patterns of HDO structures, suggesting that HDO formation is not enough to mitigate aPTT prolongation to nearly normal levels (Figure S3B). The binding of DabOs resulted in a marked decrease in the association between PS modifications in the major groove and proteins corresponding to toxicities, thereby resulting in further attenuation of aPTT prolongation and achieving nearly normalized aPTT (Figure 4C).

Dab oligomer/Chol-HDO complex ameliorates complement activation *ex vivo*

Complement pathway activation is also known as class-related toxicity of the PS-ASOs.[23,26,29] *Ex vivo* study measuring C3a levels showed high C3a levels in cynomolgus monkey serum incubated with ASOs and Chol-HDOs for two different target RNAs as well as with zymosan, which was used as a positive control for complement activation (Figure S4). The DabO/Chol-HDO complex showed significantly lower C3a levels than Chol-HDO alone, suggesting that DabO can mitigate complement activation induced by Chol-HDO.

To clarify the mechanism of ameliorating complement activation by DabO, we compared the binding properties of Chol-HDO with factor H to DabO/Chol-HDO with factor H by gel-shift assay (Figure S5). The electrophoretic mobility of factor H was shorter in the lanes where Chol-HDO and factor H were added than in the lanes where Dab12/Chol-HDO complex and factor H were added (Figures S5A–S5C), suggesting the lower binding affinity of the Dab12/Chol-HDO complex to factor H than Chol-HDO.

Pharmacokinetic and pharmacodynamic profile of low-dose Dab oligomer/Chol-HDO complex *in vivo*

We next evaluated the pharmacokinetic study of low-dose Dab12/Chol-HDO complex *in vivo* using FAM-labeled Dab12 and Alexa 568-labeled Chol-HDO complex (Figure 5A), whose fluorescent pairs were confirmed to generate FRET *ex vivo* (Figure S2). Crlj:CD1 mice were intravenously injected with 3.8 nmol of FAM-labeled Dab12/Alexa 568-labeled Chol-HDO complex (1 mg/kg as the parent ASO) at mixing molar ratio of 1:1. Serum was collected at 0.25, 0.5, 1, and 2 h after injection, and fluorescence intensity and FRET signal in serum were analyzed by the i-control instrument. The fluorescence signal of

Table 1. Summary of blood chemistry analyses in mouse serum after administration of PBS, Chol-HDO, or Dab oligomer/Chol-HDO complex

	PBS	Chol-HDO	Chol-HDO + Dab12 1:1	Chol-HDO + Dab12 1:2
T-Bil	0.053 ± 0.019	0.06 ± 0.005	0.047 ± 0.005	0.06 ± 0.005
BUN	31.9 ± 1.01	28.4 ± 1.31	36.1 ± 3.08	29.8 ± 1.85
Cre	0.123 ± 0.003	0.083 ± 0.005	0.127 ± 0.012	0.107 ± 0.005
Na	150.3 ± 0.720	150.0 ± 1.25	148.7 ± 0.272	148.0 ± 0.471
AST	72.3 ± 10.8	72.0 ± 6.53	86.0 ± 3.68	67.3 ± 9.22
ALT	23.3 ± 2.72	25 ± 2.16	26.3 ± 2.68	23.3 ± 0.981

Data are presented as the mean ± SEM; $n = 3$ per group. ALT, alanine aminotransferase; AST, aspartate aminotransferase; BUN, blood urea nitrogen; Cre, creatinine; T-Bil, total bilirubin.

Chol-HDO (Alexa 568) was high until 0.5 h after injection. In contrast, the FRET signal was decreased immediately after injection (Figure 5A). The FRET signal at 2 h after injection of Dab12/Chol-HDO complex was almost the same as that of serum from PBS-injected mice (Figure 5A, dotted line), suggesting that most Dab12 was dissociated from Chol-HDO at least 2 h after injection of low-dose Dab12/Chol-HDO complex. Next, dose-response curves of *Malat1* RNA inhibition in Crlj:CD1 mice liver 3 days after injection of Chol-HDO or Dab12/Chol-HDO complex were generated (Figure 5B). There were no significant differences in ED_{50} between mice injected with Chol-HDO and Dab12/Chol-HDO complex, suggesting that binding of Dab12 did not affect silencing efficacy of Chol-HDO in the liver.

To evaluate the safety of DabO/Chol-HDO complex treatment, we analyzed the serum levels of various biomarkers 3 days after injection of 1.6 mg/kg Chol-HDO or Dab12/Chol-HDO complex (Table 1). Liver dysfunction (alanine aminotransferase [ALT] level) or kidney dysfunction (creatinine [Cre] level) was not observed in Chol-HDO-injected mice, as previously shown.[6,7] Moreover, the complex formation of Dab12 with Chol-HDO revealed no additional toxicity, which indicates the safety of treating the DabO/Chol-HDO complex.

Distribution of Dab oligomer/Chol-HDO complex in liver

To assess when dissociation of the complex would occur in tissues, we analyzed confocal laser scanning microscopy images of mouse livers (Figures 5C and 5D) using FAM-labeled Dab12 and Alexa 647-labeled Chol-HDO. At 0.5 h after injection of 3.8 nmol of FAM-labeled Dab12/Alexa 647-labeled Chol-HDO complex (1 mg/kg), the fluorescence signal of Dab12 (green) colocalized with that of the parent ASO (red) in the hepatocytes (arrows) as well as non-parenchymal cells (Figure 5C). The images indicated that a part of Dab12/Chol-HDO complexes was taken by hepatocytes in the form of the complex. On the contrary, the signal of FAM-Dab12 was not observed at 3 h after injection, while the parent ASO fluorescence signal was observed in the hepatocytes (arrowheads) as well as non-parenchymal cells (Figure 5D). These findings suggested that DabO/Chol-HDO complex was delivered to hepatocytes as a complex within 0.5 h after administration and that DabO was dissociated from Chol-HDO in the cells.

Pharmacokinetic and pharmacodynamic profile of high-dose Dab oligomer/Chol-HDO complex *in vivo*

To evaluate the pharmacokinetics of high-dose DabO/Chol-HDO complex *in vivo*, C57BL/6 mice were intravenously injected with 189 nmol of Chol-HDO (50 mg/kg as the parent ASO) or 189 nmol of Dab8/Chol-HDO complex at mixing molar ratio of 2:1 (50 mg/kg as the parent ASO), and the ASO concentration-time profiles in plasma were evaluated. Plasma concentration of the parent ASO in Dab8/Chol-HDO-injected mice was lower than that in Chol-HDO-injected mice (Figure 6A). Next, we evaluated the effect of DabOs on the gene-silencing efficacy of high-dose Chol-HDO *in vivo*. As for Dab12/Chol-HDO complex, visible aggregation was observed at a mixing molar ratio of 2:1 (mixing of 800 μM of 236 μL Chol-HDO with 5 mM of 75.6 μL Dab12), and thus only Dab12/Chol-HDO (1:1) was evaluated. This aggregation was not observed in the lower concentrations of Dab12 and Chol-HDO used in Figure 5 or Figures 6E and 6F. An excess amount of DabOs may cause aggregation with Chol-HDO due to both the hydrophobicity of cholesterol ligand and electrostatic interaction at high concentrations. There was no noticeable difference in gene-silencing effects on *Malat1* RNA among the groups in liver and kidney (Figures 6B and 6C). Importantly, DabO/Chol-HDO was similarly effective as Chol-HDO for regulating the target gene in the brain (Figure 6D). The Dab10/Chol-HDO complex also exhibited a gene-silencing efficacy similar to that of Chol-HDO (Figure S6). These results indicated that complex formation with DabOs does not interfere with the gene-silencing effect and BBB-crossing property of Chol-HDO.

Next, we evaluated the effects of the high-dose DabO/Chol-HDO complex on the class-related toxicities *in vivo*. C57BL/6 mice were intravenously injected with 75.6 nmol of Chol-HDO (20 mg/kg as the parent ASO) or 75.6 nmol of DabOs/Chol-HDO complex (20 mg/kg as the parent ASO). Dab12/Chol-HDO complex at a mixing molar ratio of 2:1 did not show aggregation in this dose (mixing 600 μM of 126 μL Chol-HDO with 1 mM of 151.2 μL Dab12). Plasma was then collected 30 min after injection, and aPTT was analyzed. Dab10/Chol-HDO complex (2:1) showed significantly shorter aPTT than Chol-HDO, and Dab12/Chol-HDO complex (2:1) accomplished nearly normalized aPTT (Figure 6E). These results indicated that DabOs/Chol-HDO complex also mitigates aPTT prolongation *in vivo* as well as *ex vivo*. We also evaluated the effects of the DabO/Chol-HDO complex on thrombocytopenia. C57BL/6 mice were intravenously injected with 75.6 nmol of Chol-HDO or 75.6 nmol of Dab12/Chol-HDO complex (1:2). Blood was collected 6 h after injection, and platelet count was analyzed. Dab12/Chol-HDO complex partially ameliorated thrombocytopenia induced by high-dose administration of Chol-HDO (Figure 6F).

Dab oligomer/HDO complex prevents acute-phase toxicity and focal necrosis in brain section after high-dose intravenous injection of Chol-HDO

High-dose intravenous administration of Chol-HDO (189 nmol, 50 mg/kg as the parent ASO) in C57BL/6 mice revealed acute

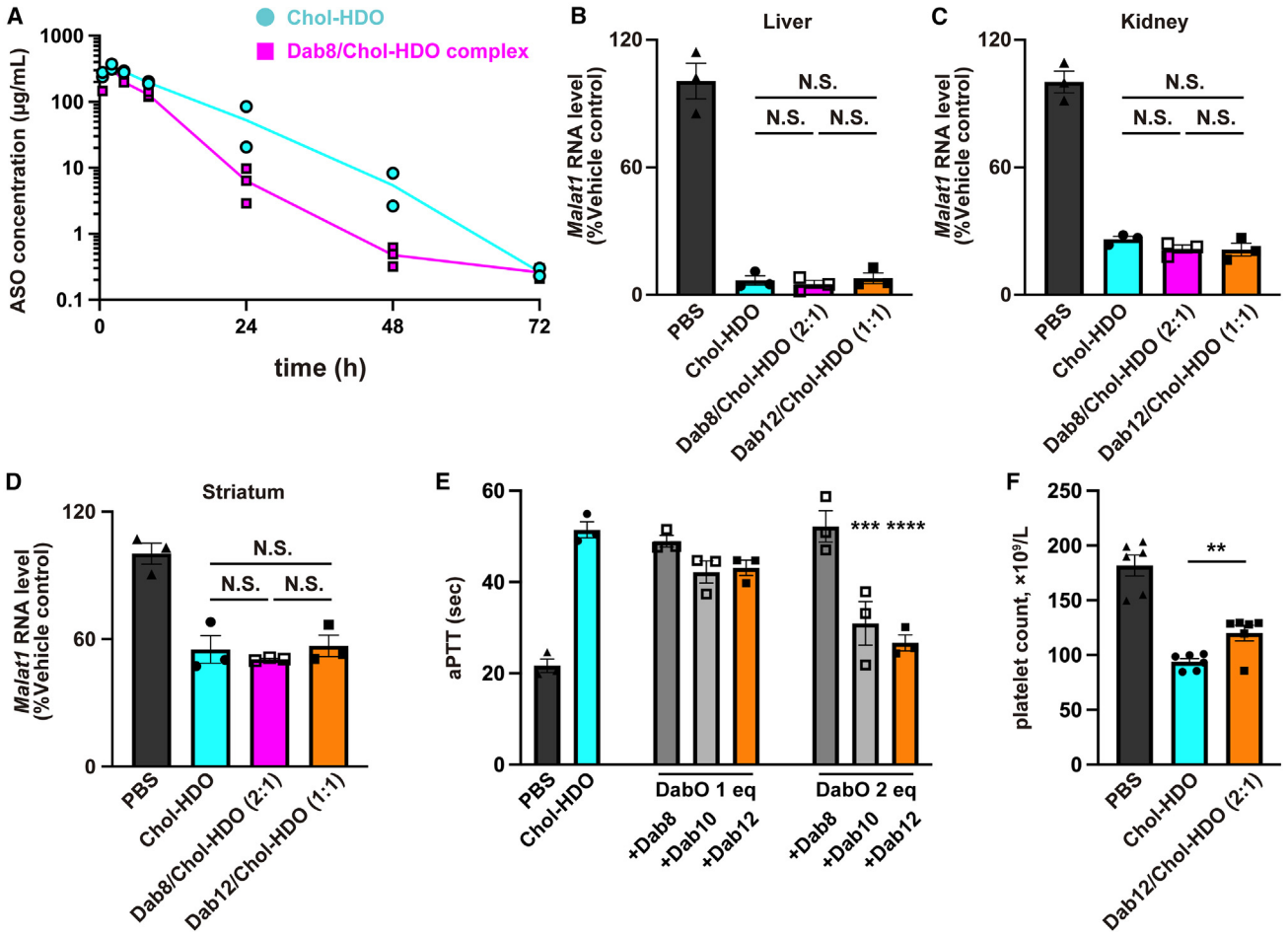

Figure 6. Pharmacokinetics, pharmacodynamics, and toxicological study after administration of high-dose Chol-HDO or Dab oligomer/Chol-HDO complex

(A) Plasma concentrations of the parent ASO at 0.5, 2, 4, 8, 24, 48, or 72 h after intravenous injection in C57BL/6 mice with 189 nmol of Chol-HDO or Dab8/Chol-HDO complex (50 mg/kg as the parent ASO) targeting mouse *Malat1* RNA. (B–D) *Malat1* RNA expression levels in mouse liver (B), kidney (C), and brain (D) were measured by RT-qPCR 3 days after injection of Chol-HDO or Dab8/Chol-HDO complex. ANOVA followed by Tukey's test was conducted for the four groups. (E) aPTT in mice intravenously injected with 75.6 nmol of 16-mer Chol-HDO or Dab/Chol-HDO complex (20 mg/kg as the parent ASO) targeting *Malat1* RNA at 30 min after injection. ANOVA followed by Dunnett's test was conducted for Chol-HDO and DabO/Chol-HDO-injected groups. (F) Platelet count in mice intravenously injected with 75.6 nmol of 16-mer Chol-HDO or Dab12/Chol-HDO complex (20 mg/kg as the parent ASO) targeting *Malat1* RNA at 6 h after injection. Student's t test was conducted. Data are presented as mean (A) or mean ± SEM (B–F); $n = 2$, 3 (A–E), or 6 (F) per group; N.S., not significant; $^{**}p < 0.01$, $^{***}p < 0.001$, $^{****}p < 0.0001$ compared to Chol-HDO.

toxicities. We assessed behavioral abnormalities 0.5 h after injection using the hunched posture scoring system and the mouse grimace scale.[30,31] Chol-HDO-injected mice presented clinical signs of hypoactivity and hunched posture, leading to high scores of these scoring systems (Figures 7A and 7B), although they disappeared within 2 h after injection. The complex formation with Dab8 (2:1) significantly improved these behavioral abnormalities compared to Chol-HDO only (Figures 7A and 7B). Histopathological study showed focal necrosis in the cerebral cortex, hippocampus, inferior colliculus, and cerebellum in Chol-HDO-injected mice (Figure 7D). On the other hand, no evident abnormal findings were observed mice injected with 5% dextrose vehicle (Figure 7C) and Dab8/Chol-HDO complex (Figure 7E).

DISCUSSION

We confirmed that class-related toxicities of HDOs were significantly less severe than those of ASOs. These advantages of HDOs in toxicities may be attributed to their substantially decreased non-specific binding activity to serum molecules compared to ASOs.[32] However, despite reducing non-specific binding to serum proteins by HDO structure, Chol-HDOs still exhibited some class-related toxicities, especially *in vivo*. This study demonstrates that binding of DabOs to Chol-HDOs can further mitigate these class-related toxicities and prevent acute-phase behavioral abnormalities and focal brain necrosis induced by high-dose administration of Chol-HDOs.

PS-ASOs show high binding affinity to the target RNAs and increased binding potentials to proteins.[33] Although PS

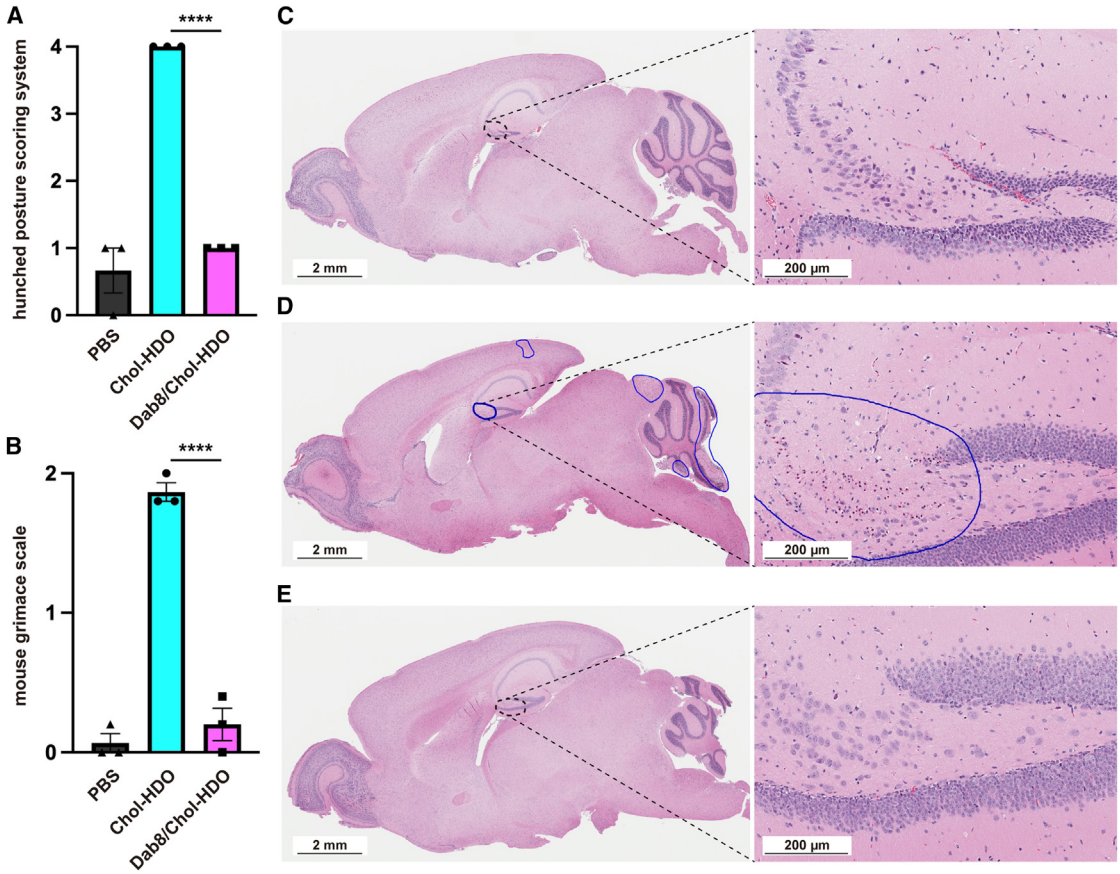

Figure 7. Histopathological analysis after administration of high-dose Chol-HDO or Dab oligomer/Chol-HDO complex

(A and B) Hunched posture scoring system (A) and mouse grimace scale (B) 0.5 h after high-dose systemic administration of Chol-HDO or DabO/Chol-HDO complex. (C–E) Representative H&E staining of brain sections from mice injected with 5% dextrose (C), Chol-HDO (D), or Dab8/Chol-HDO complex (mixing molar ratio = 2:1) (50 mg/kg as the parent ASO) (E) at 3 days after injection. Histopathological analysis revealed focal necrosis in the cerebral cortex, hippocampus, inferior colliculus, and cerebellum (blue circle) in Chol-HDO-injected mice (D). No abnormal findings were observed in PBS-injected (C) or Dab8/Chol-HDO complex-injected (E) mice. Scale bars represent 2 mm for the panels on the left and 200 μm for those on the right. $n = 3$ (A and B) per group; ***$p < 0.001$, ****$p < 0.0001$ compared to Chol-HDO. In (A) and (B), only the statistical comparison between Chol-HDO and Dab8/Chol-HDO complex among the multiple comparisons is described.

modification increases nuclease stability resulting in better efficacy, non-specific binding between PS-ASOs and serum/cellular proteins causes various toxicities.[34] Here, we showed that some toxicities of PS-ASOs can be ameliorated by HDO formation because HDO structure hides PS modifications in the parent ASO strand in HDO's major groove, resulting in decreased binding to serum proteins.[32] However, aPTT prolongation could not be normalized by HDO formation even with various locations of PS modifications, suggesting that HDO formation is insufficient to normalize aPTT. DabOs specifically bind to the PS modifications in the major groove of Chol-HDOs, which can strongly inhibit the interaction between PS modifications in the major groove and serum proteins. Therefore, the antidote effects of DabOs presented in the current study are probably mediated by the further decreased non-specific interaction of the DabO/Chol-HDO complex with serum proteins related to toxicities, combined with the effect of HDO structure.

The conjugation of a cholesterol ligand increases binding affinities to various proteins in the blood.[35] The cholesterol conjugation to ASOs or HDOs extends their blood retention after systemic injection,[7] which probably emphasizes some toxicities. Indeed, cholesterol-conjugated ASOs cause some lethal toxicities,[36] and Chol-HDOs show more pronounced aPTT prolongation (Figure 6E) *in vivo*. The DabOs/Chol-HDO complex still showed high blood retention *in vivo* (Figure 6A) while reducing the acute toxicities. Taken together, complex formation with DabOs reduces PS modification-related toxicities while maintaining high blood retention attributed to the cholesterol ligand.

We demonstrated that HDOs and Chol-HDOs with PS modifications caused aPTT prolongation and complement activation, as did the parent ASOs, suggesting the same mechanism underlying the toxicities of HDOs as ASOs. Complement activation is reported as one of the non-specific protein-binding effects of ASOs.[26,29] Complement

activation is mediated by the direct interaction of PS-ASOs with plasma factor H, a negative regulator of the alternative pathway cascade.[26] Factor H has polyanion binding sites,[37,38] and the electrostatic interaction between factor H and PS-ASOs leads to the sequestration of factor H, which promotes activation in this pathway. In this study, we demonstrated the lower binding affinity of HDO to factor H than ASO and the lower binding affinity of Chol-HDO to factor H than DabO/Chol-HDO. Together, HDO structure with DabO mitigates complement activation by reducing the binding affinity to factor H. Complement activation may not be a critical problem in developing oligonucleotide therapeutics because it is rarely observed in humans.[26] However, our results about the antidote effect of DabOs on complement activation emphasize the utility of DabOs in reducing the toxicities of Chol-HDO induced by electrostatic binding with proteins.

The same mechanism, that is, reduced protein binding of Chol-HDO by DabOs, possibly also underlies the mitigation of other toxicities. The aPTT prolongation by PS-ASOs is mediated by inhibition of the intrinsic tenase complex and takes place in a PS-related manner.[24,25] DabO/Chol-HDO complex has fewer PS modifications that can interact with proteins because the protonated amino groups of the DabO bind to the phosphates of Chol-HDO, which may decrease the interaction with the intrinsic tenase complex and therefore reduce aPTT prolongation. Thrombocytopenia caused by systemic injection of high-dose ASOs has been reported as an adverse effect in clinical trials.[4,39] Interactions between PS-ASOs and some proteins, such as platelet collagen receptor glycoprotein (GPVI) and platelet factor 4 (PF4), are associated with thrombocytopenia in a PS-related manner.[40–42] GPVI has positively charged basic residues lining a groove on domain D1 with which negatively charged ASOs can interact,[40] and PF4 is also a positively charged protein known to be associated with heparin-induced thrombocytopenia.[43] It is hence speculated that the DabO/Chol-HDO complex has fewer PS modifications to electrostatically interact with GPVI or PF4 because DabOs bind to the phosphates of Chol-HDO, resulting in the mitigating effect on thrombocytopenia. These toxicities might be prevented by subcutaneous administration,[7] but subcutaneous injection sometimes causes severe skin disorders,[44] and the permissible amount of drugs is limited.[45] Complex formation with DabOs can be one of the alternatives to overcome the acute side effects of Chol-HDO.

Importantly, complex formation with DabOs did not interfere with the gene-silencing efficacy of Chol-HDO. Although many chemical modifications effectively overcome the toxicities of PS-ASOs,[46–48] detailed modifications were needed to maintain their silencing efficacies. These reports also indicate the trade-off relationship between gene-silencing efficacies and toxicities when ASO backbones or 2′ position of the ribose sugars were chemically modified. On the other hand, DabO is an oligopeptide that does not properly bind to single-stranded ASO but specifically interacts with the A-type double-helical structure of Chol-HDO, representing an alternative approach to reducing the adverse effects of oligonucleotide therapeutics. Furthermore, the non-covalent binding of DabOs to the phosphates enables the separation of the DabO/Chol-HDO complex *in vivo* within a few hours after administration. Although some DabO/Chol-HDO complexes were delivered to hepatocytes in complex forms (Figure 5A), the DabO/Chol-HDO complex could be dissociated in the cells because the parent ASO strand and cRNA strand of HDO are separated at the early endosomes.[8] After the dissociation of the DabO/Chol-HDO complex, the parent ASO strand would escape from the endosome and be transported to the nucleus. At the same time, DabO is possibly degraded in the late endosome or lysosome. Based on these intracellular processes, DabOs do not disturb the gene-silencing efficacy of Chol-HDO. In addition, DabOs show the advantage of not interfering with the potency of conjugated delivery ligands at the 5′ terminus of the cRNA strand of HDOs. The enhanced delivery to the liver or the BBB-crossing ability is a distinctive feature of lipid-conjugated HDO,[6,7] and these advantages depend on the lipid ligands.[7] We demonstrated that the DabO/Chol-HDO complex could cross the BBB and effectively suppress CNS genes, indicating that DabOs do not interfere with the BBB-crossing property of cholesterol ligands.

Notably, the mitigation of the toxicities of Chol-HDOs was accomplished with a small amount of cation by using DabOs. In this study, the N/P ratio is 0.8, even in the 1:2 complex of Chol-HDO and Dab12. On the other hand, most conventional oligo-/polycationic molecules used in the complex with oligonucleotide-based drugs are used with an N/P ratio of much more significant than 1, which means that large excess amounts of cation are used.[19,20,49,50] Since a high N/P ratio potentially leads to toxicity deriving from such cationic molecules,[19,20] improving the properties of oligonucleotide-based drugs with a small amount of cation is advantageous for their safety and druggability. Unlike most conventional cationic molecules, DabOs are designed to specifically bind to the major groove of A-type double-helical structure, including HDO. Therefore, it is reasonable that their specific binding with high affinity to HDO is the key to mitigating the toxicities of Chol-HDO with an N/P ratio of less than 1.

This study has some limitations. First, the effects of DabO on the toxicity were evaluated for a few sequences, *Malat1*, *Dmpk*, and *SOD1*. DabO showed a favorable impact on aPTT prolongation, although the degree of the effect varied by sequence (Figure 4). These variations are probably because sequence-dependent mechanisms other than PS modifications are related to aPTT prolongation while DabO reduced only PS modification-related toxicities. Second, the binding affinity between DabOs and Chol-HDO was assessed in only a few sequences. Based on our gel electrophoresis results, the binding affinity may vary depending on the base length of Chol-HDO and the length of DabOs, which should be further studied to lead to the consequences. Finally, our study did not directly compare the mitigating effects of the toxicities between DabO and backbone or sugar modifications. However, DabOs do not interfere with the activity while mitigating toxicities and can be used together with other chemical modifications such as backbone modifications, emphasizing their potential to reduce the toxicities of oligonucleotide therapeutics.

In summary, our study demonstrated that the ASO class-related toxicities could be ameliorated by HDO formation despite the increased number of PS modifications. Moreover, complex formation with duplex-specific DabOs further mitigates these toxicities by maintaining a high gene-silencing efficacy of Chol-HDOs in many tissues, including the brain. These antidote effects are probably due to preventing non-specific protein bindings of Chol-HDOs. DabOs can be an alternative approach for reducing toxicities of oligonucleotide therapeutics with duplex structure, which is entirely different from the conventional approaches.

MATERIALS AND METHODS

Design and synthesis of oligonucleotides

A series of oligonucleotides were synthesized by GeneDesign (Osaka, Japan). The sequence and modifications of ASOs and cRNAs used in this study are listed in Table S1. To generate HDO, we hybridized equimolar concentrations of ASOs and cRNAs by denaturing them at 95°C for 5 min and slowly cooling (1°C/min) to 37°C to anneal them.

Synthesis of Dab/HDO complexes

Dab oligomers were synthesized by Scrum (Tokyo, Japan) and Toray Research Center (Tokyo, Japan). A tripeptide of glycine, glycine, and tyrosine was conjugated to Dab oligomers to evaluate their amounts easily. DabOs were diluted with PBS. Ligand-conjugated HDOs were bound with DabOs in molar ratios (ligand-conjugated HDOs/DabOs) ranging from 1:1 to 1:3 by incubating them at room temperature for at least 30 min.

UV melting analysis

Absorbance-versus-temperature profile measurements were conducted. All the experiments were conducted in 10 mM phosphate buffer containing 100 mM NaCl at pH 7.0. The concentration of Chol-HDO was 5 μM. The UV absorbance at both 260 and 320 nm was monitored with the temperature. The samples were rapidly heated to 95°C, maintained at this temperature for 20 min, and finally allowed to cool to room temperature at a rate of 0.5°C/min. The dissociation was recorded by heating the samples to 95°C at a rate of 0.5°C/min.

Mouse experiments

For the mouse experiments presented in Figures 1, 5, 6E, and 6F, and Table 1, 5-week-old wild-type male Crlj:CD1 (ICR) mice were obtained from Oriental Yeast (Tokyo, Japan). For the mouse experiments presented in Figures 6A–6D and 7, 12-week-old wild-type male C57BL/6J mice were obtained from Charles River, Japan (Kanagawa, Japan). These mice were maintained on a 12:12-h light/dark cycle in a pathogen-free animal facility with free access to food and water. HDOs were administered to mice via the tail vein. All oligonucleotides were diluted with PBS or 5% dextrose. For the mouse experiments presented in Figures 1, 5, 6E, and 6F, and Table 1, mice were anesthetized with 4% isoflurane and euthanized by transcardial perfusion with PBS. For the mouse experiments presented in Figures 6A–6D and 7, mice were euthanized by decapitation. All protocols followed the ethics and safety guidelines for animal experimentation and were approved by the Ethics Committee of Tokyo Medical and Dental University (#A2022-085A) or the Institutional Animal Care and Use Committee of Shonan Health Innovation Park (#AU-00020599).

Electrophoresis analysis

Twenty picomoles of ASO, Chol-HDO, DabO/Chol-HDO complex, or Lys12/Chol-HDO complex, were diluted in PBS to make a 10-μL volume of the mixture. Two microliters of 10% sucrose buffer was used as a loading buffer to avoid the possible effects of dye-containing loading buffers. The mixture was loaded onto a non-denaturing bisacrylamide 16% gel with Tris-borate-EDTA buffer for 3 h at 100 V. After electrophoresis, acrylamide gel was incubated with GelRed (Wako Pure Chemical Industries, Osaka, Japan) for 15 min, and an image was acquired with a ChemiDoc system (Bio-Rad, Hercules, CA, USA). K_D values were calculated according to the previous paper.[28] The exposure time was 1.6 s for Figures 3C, 3E, S1C, and S1D, 8.0 s for the Alexa 488 filter in Figures 3B, and 1.0 s for the Alexa 647 filter in Figure 3B.

FRET analysis

The energy transfer reaction between DabO and Chol-HDO was evaluated by FRET analysis using an i-control instrument (Tecan). Fluorescence intensity was measured at 518 and 603 nm with excitation at 492 nm. The FRET signal was defined as the fluorescence intensity ratio: [intensity at 603 nm]/[intensity at 518 nm]. The energy transfer reaction *in vivo* was also evaluated by FRET analysis. Serum from mice injected with FAM-labeled Dab12/Alexa 568-labeled Chol-HDO complex was collected 15, 30, 60, and 120 min after the injection. First, serum was obtained, after which FRET signals were analyzed using the aforementioned methods.

aPTT assays

Activated partial thromboplastin time (aPTT) was analyzed by validated methods using CA50 (Sysmex, Kobe, Japan) ($n = 3$ per group). For *ex vivo* study, oligonucleotides or DabO/Chol-HDO complexes were added to pooled human plasma (George King Bio-Medical, Overland Park, KS, USA) and vortexed, then incubated for 3 min at 37°C. The same lot number of human plasma was used for all the *ex vivo* assays. For *in vivo* study, collected mouse plasma was incubated for 3 min at 37°C. After the incubation, 0.05 mL of thrombocheck-APTT-SLA (Sysmex) was added and incubated for 1 min, followed by the addition of 0.025 mol/L $CaCl_2$ (0.05 mL) and incubation for 2 min, before determining the clotting time.

Complement activation assays

Complement activation in cynomolgus monkey serum samples (KAC, Kyoto, Japan) was evaluated by MicroVue C3a Plus (Quidel, San Diego, CA, USA). Dilutions of oligonucleotides or peptide-HDO complexes were added to serum at a 1:10 to 1:20 ratio, v/v. For *in vitro* complement activation studies, oligonucleotides or DabOs/Chol-HDO complexes were incubated with monkey serum at 37°C for 45 min. Activation was terminated by placing the aliquots

in a container of crushed ice. Zymosan (2.5 mg/mL) (Nacalai Tesque, Tokyo, Japan) was used as a positive control.

Fluorescence polarization assays

Native human factor H (Sigma-Aldrich, Burlington, MA, USA) and Alexa 647-labeled nucleic acids were incubated at 37°C for 30 min. Complexes were excited with polarized light at 635 nm, and emission light at 670 nm was measured as fluorescence polarization signals (Tecan). K_D values were calculated with GraphPad Prism 9 software (GraphPad Software, San Diego, CA, USA).

Gel-shift assays

Chol-HDO or Dab12/Chol-HDO complex (20 pmol) was added to 0–50 pmol of native human factor H (Sigma-Aldrich), and the mixtures were incubated at 37°C for 30 min. The samples were resolved by electrophoresis on a 4%–20% gradient gel (Bio-Rad) for 60 min at 100 V. The gels were then stained by Coomassie brilliant blue (Nacalai Tesque,). An image was acquired with a ChemiDoc system (Bio-Rad). The exposure time was 0.6 s.

RNA extraction and RT-qPCR

RNA was extracted from culture cells and mouse tissues using the MagNA Pure 96 system (Roche Diagnostics, Penzberg, Germany) or Isogen (Nippon Gene, Tokyo, Japan). Isolated total RNA was reverse-transcribed with Takara 5× Prime Script RT Master Mix (Takara Bio, Shiga, Japan) followed by real-time qPCR analysis with the Light Cycler 480 Real-Time PCR Instrument (Roche Diagnostics). The results were normalized against β-actin (*Actb*) mRNA. Primer sequences for *Malat1* RNA and *Actb* mRNA were identical to those in our previous paper.[7]

Histopathological analyses

For pathological analyses of brain tissue, mice were injected with 50 mg/kg Chol-HDO or Dab8-Chol-HDO complex. Mice were euthanized 3 days after injection. After euthanasia, organs were postfixed in 4% paraformaldehyde (PFA) (FUJIFILM Wako Pure Chemical, Osaka, Japan) in PBS for 6 days, embedded in paraffin, cut into 3-μm-thick sections using gliding microtome TU-213 (Yamato Koki, Saitama, Japan), and stained with hematoxylin (Merck, Darmstadt, Germany) and eosin (FUJIFILM Wako Pure Chemical). To analyze the biodistribution of peptide-Chol-HDO complex, mice were injected with the complex of 1 mg/kg Alexa 647-labeled Chol-HDO and equimolar concentrations of Dab oligomer. Mice were euthanized at 30 min or 3 h after injection. After euthanasia, organs were postfixed in 4% PFA (Wako Pure Chemical Industries) in PBS for 24 h, rapidly frozen, and cut into 10-μm-thick sections using a Leica CM 3050S cryostat (Leica Microsystems, Wetzlar, Germany). The sections were stained with DAPI (Vector Laboratories, Newark, CA, USA) to visualize nuclei and Alexa Fluor 568 phalloidin (Thermo Fisher Scientific, Waltham, MA, USA) to visualize cell membranes. The slides were analyzed using a Nikon A1R laser scanning confocal microscopy (Nikon, Tokyo, Japan).

Determination of parent ASO plasma concentrations

Parent ASO in plasma samples was extracted using a phenol-chloroform liquid-liquid extraction method and analyzed by liquid chromatography-tandem mass spectrometry (LC-MS/MS). MS was performed using a Sciex API 4000 instrument (Sciex, Framingham, MA, USA) with an electrospray ionization source (Applied Biosystems, Waltham, MA, USA/Sciex).

Statistical analysis

All data represent mean ± standard error of the mean (SEM) unless otherwise mentioned. Differences among more than three groups were analyzed by one-way analysis of variance (ANOVA) with post hoc Tukey's test for Figures 1D–1F, 5B, 6B–6D, 6F, 7A, and 7B, or ANOVA with post hoc Dunnett's correction for Figures 4B–4F and 6E for multiple comparisons. Statistical differences between the two groups were analyzed by Student's t test. The significance criterion was set at $p < 0.05$. All statistical analyses were performed using GraphPad Prism 9 software.

DATA AND CODE AVAILABILITY

The authors declare that all data supporting the findings of this study are available within the paper and supplemental information. Source data are available from the corresponding author upon reasonable request.

SUPPLEMENTAL INFORMATION

Supplemental information can be found online at https://doi.org/10.1016/j.omtn.2024.102289.

ACKNOWLEDGMENTS

We thank Kensuke Ihara (Tokyo Medical and Dental University) for his technical support. We also thank Satoko Yoshioka (Takeda Pharmaceutical) for histopathological evaluation, as well as Ikumi Chisaki and Hisashi Fujita (Takeda Pharmaceutical) for pharmacokinetic analysis. This research was supported by grants from the Core Research for Evolutional Science and Technology (CREST, JPMJCR12L4) and the Japan Science and Technology Agency, Japan to T.Y. This research was also supported by the Basic Science and Platform Technology Programs for Innovative Biological Medicine (18am0301003h0005) and Advanced Biological Medicine (20am0401006h0002) to T.Y., from the Japan Agency for Medical Research and Development (AMED; Tokyo, Japan), and a JSPS KAKENHI Grant-in-Aid for Scientific Research (A) (19H01016 to T.N. and T.Y.), (A) (22H00440 to T.N.), and (C) (19K06993 to R. I. H.) from the Ministry of Education, Culture, Sports, Science and Technology of Japan (MEXT) (Tokyo).

AUTHOR CONTRIBUTIONS

M.O., T.N., R.I.H., K.S., Y.M., T.W., and T.Y. conceived the concept of Dab oligomer/Chol-HDO complex. M.O., T.N., R.I.H., K.M., T.T., M.N., and T.Y. designed the study. M.O., K.Y.-T., N.T., K.T., K.S., T.T., M.N., and K.T. performed the experiments. M.O., T.N., R.I.H., and T.Y. wrote the manuscript.

DECLARATION OF INTERESTS

T.Y. collaborates with Daiichi Sankyo Co., Ltd., Rena Therapeutics, Inc., Takeda Pharmaceutical Co., Ltd., and Toray Industries, Inc., and serves as the academic adviser for Rena Therapeutics, Inc. and Braizon Therapeutics, Inc. T.T., M.N., and K.M. are paid employees of Takeda Pharmaceutical Co., Ltd. M.O., T.N., R.I.H., K.T., K.S., Y.M., T.W., and T.Y. are inventors of patents describing the peptides used in this study (WO2020262555A1).

REFERENCES

1. Yacyshyn, B.R., Bowen-Yacyshyn, M.B., Jewell, L., Tami, J.A., Bennett, C.F., Kisner, D.L., and Shanahan, W.R., Jr. (1998). WR. A placebo-controlled trial of ICAM-1 antisense oligonucleotide in the treatment of Crohn's disease. Gastroenterology *114*, 1133–1142.
2. Henry, S.P., Bolte, H., Auletta, C., and Kornbrust, D.J. (1997). Evaluation of the toxicity of ISIS 2302, a phosphorothioate oligonucleotide, in a four-week study in cynomolgus monkeys. Toxicology *120*, 145–155.
3. Galbraith, W.M., Hobson, W.C., Giclas, P.C., Schechter, P.J., and Agrawal, S. (1994). Complement activation and hemodynamic changes following intravenous administration of phosphorothioate oligonucleotides in the monkey. Antisense Res. Dev. *4*, 201–206.
4. Crooke, S.T., Baker, B.F., Witztum, J.L., Kwoh, T.J., Pham, N.C., Salgado, N., McEvoy, B.W., Cheng, W., Hughes, S.G., Bhanot, S., and Geary, R.S. (2017). The effects of 2'-O-methoxyethyl containing antisense oligonucleotides on platelets in human clinical trials. Nucleic Acid Therapeut. *27*, 121–129.
5. Frazier, K.S. (2015). Antisense oligonucleotide therapies: the promise and the challenges from a toxicologic pathologist's perspective. Toxicol. Pathol. *43*, 78–89.
6. Nishina, K., Piao, W., Yoshida-Tanaka, K., Sujino, Y., Nishina, T., Yamamoto, T., Nitta, K., Yoshioka, K., Kuwahara, H., Yasuhara, H., et al. (2015). DNA/RNA heteroduplex oligonucleotide for highly efficient gene silencing. Nat. Commun. *6*, 7969.
7. Nagata, T., Dwyer, C.A., Yoshida-Tanaka, K., Ihara, K., Ohyagi, M., Kaburagi, H., Miyata, H., Ebihara, S., Yoshioka, K., Ishii, T., et al. (2021). Cholesterol-functionalized DNA/RNA heteroduplexes cross the blood-brain barrier and knock down genes in the rodent CNS. Nat. Biotechnol. *39*, 1529–1536.
8. Ono, D., Asada, K., Yui, D., Sakaue, F., Yoshioka, K., Nagata, T., and Yokota, T. (2021). Separation-related rapid nuclear transport of DNA/RNA heteroduplex oligonucleotide: unveiling distinctive intracellular trafficking. Mol. Ther. Nucleic Acids *23*, 1360–1370.
9. Finkel, R.S., Mercuri, E., Darras, B.T., Connolly, A.M., Kuntz, N.L., Kirschner, J., Chiriboga, C.A., Saito, K., Servais, L., Tizzano, E., et al. (2017). Nusinersen versus sham control in infantile-onset spinal muscular atrophy. N. Engl. J. Med. *377*, 1723–1732.
10. Miller, T.M., Pestronk, A., David, W., Rothstein, J., Simpson, E., Appel, S.H., Andres, P.L., Mahoney, K., Allred, P., Alexander, K., et al. (2013). An antisense oligonucleotide against SOD1 delivered intrathecally for patients with SOD1 familial amyotrophic lateral sclerosis: a phase 1, randomised, first-in-man study. Lancet Neurol. *12*, 435–442.
11. Tabrizi, S.J., Leavitt, B.R., Landwehrmeyer, G.B., Wild, E.J., Saft, C., Barker, R.A., Blair, N.F., Craufurd, D., Priller, J., Rickards, H., et al. (2019). Targeting huntingtin expression in patients with Huntington's disease. N. Engl. J. Med. *380*, 2307–2316.
12. DeVos, S.L., Miller, R.L., Schoch, K.M., Holmes, B.B., Kebodeaux, C.S., Wegener, A.J., Chen, G., Shen, T., Tran, H., Nichols, B., et al. (2017). Tau reduction prevents neuronal loss and reverses pathological tau deposition and seeding in mice with tauopathy. Sci. Transl. Med. *9*, eaag0481.
13. Sullivan, J.M., Mazur, C., Wolf, D.A., Horky, L., Currier, N., Fitzsimmons, B., Hesterman, J., Pauplis, R., Haller, S., Powers, B., et al. (2020). Convective forces increase rostral delivery of intrathecal radiotracers and antisense oligonucleotides in the cynomolgus monkey nervous system. J. Transl. Med. *18*, 309.
14. Mazur, C., Powers, B., Zasadny, K., Sullivan, J.M., Dimant, H., Kamme, F., Hesterman, J., Matson, J., Oestergaard, M., Seaman, M., et al. (2019). Brain pharmacology of intrathecal antisense oligonucleotides revealed through multimodal imaging. JCI Insight *4*, e129240.
15. Maeda, Y., Iwata, R., and Wada, T. (2013). Synthesis and properties of cationic oligopeptides with different side chain lengths that bind to RNA duplexes. Bioorg. Med. Chem. *21*, 1717–1723.
16. Maeda, Y., Iwata Hara, R., Nishina, K., Yoshida-Tanaka, K., Sakamoto, T., Yokota, T., and Wada, T. (2019). Artificial cationic peptides that increase nuclease resistance of siRNA without disturbing RNAi activity. Nucleos Nucleot. Nucleic Acids *38*, 338–348.
17. Hara, R.I., Hisada, Y., Maeda, Y., Yokota, T., and Wada, T. (2018). Artificial cationic oligosaccharides for heteroduplex oligonucleotide-type drugs. Sci. Rep. *8*, 4323.
18. Hara, R.I., Maeda, Y., Fujimaki, H., and Wada, T. (2018). Correction: Enhancement in RNase H activity of a DNA/RNA hybrid duplex using artificial cationic oligopeptides. Chem. Commun. *54*, 11499.
19. Zhu, J., Qiao, M., Wang, Q., Ye, Y., Ba, S., Ma, J., Hu, H., Zhao, X., and Chen, D. (2018). Dual-responsive polyplexes with enhanced disassembly and endosomal escape for efficient delivery of siRNA. Biomaterials *162*, 47–59.
20. Cabral, H., Miyata, K., Osada, K., and Kataoka, K. (2018). Block Copolymer Micelles in Nanomedicine Applications. Chem. Rev. *118*, 6844–6892.
21. Watanabe, S., Hayashi, K., Toh, K., Kim, H.J., Liu, X., Chaya, H., Fukushima, S., Katsushima, K., Kondo, Y., Uchida, S., et al. (2019). In vivo rendezvous of small nucleic acid drugs with charge-matched block catiomers to target cancers. Nat. Commun. *10*, 1894.
22. Lv, H., Zhang, S., Wang, B., Cui, S., and Yan, J. (2006). Toxicity of cationic lipids and cationic polymers in gene delivery. J. Contr. Release *114*, 100–109.
23. Webb, M.S., Tortora, N., Cremese, M., Kozlowska, H., Blaquiere, M., Devine, D.V., and Kornbrust, D.J. (2001). Toxicity and toxicokinetics of a phosphorothioate oligonucleotide against the c-myc oncogene in cynomolgus monkeys. Antisense Nucleic Acid Drug Dev. *11*, 155–163.
24. Henry, S.P., Novotny, W., Leeds, J., Auletta, C., and Kornbrust, D.J. (1997). Inhibition of coagulation by a phosphorothioate oligonucleotide. Antisense Nucleic Acid Drug Dev. *7*, 503–510.
25. Sheehan, J.P., and Lan, H.C. (1998). Phosphorothioate oligonucleotides inhibit the intrinsic tenase complex. Blood *92*, 1617–1625.
26. Henry, S.P., Jagels, M.A., Hugli, T.E., Manalili, S., Geary, R.S., Giclas, P.C., and Levin, A.A. (2014). Mechanism of alternative complement pathway dysregulation by a phosphorothioate oligonucleotide in monkey and human serum. Nucleic Acid Therapeut. *24*, 326–335.
27. McCampbell, A., Cole, T., Wegener, A.J., Tomassy, G.S., Setnicka, A., Farley, B.J., Schoch, K.M., Hoye, M.L., Shabsovich, M., Sun, L., et al. (2018). Antisense oligonucleotides extend survival and reverse decrement in muscle response in ALS models. J. Clin. Invest. *128*, 3558–3567.
28. Heffler, M.A., Walters, R.D., and Kugel, J.F. (2012). Using electrophoretic mobility shift assays to measure equilibrium dissociation constants: GAL4-p53 binding DNA as a model system. Biochem. Mol. Biol. Educ. *40*, 383–387.
29. Henry, S.P., Seguin, R., Cavagnaro, J., Berman, C., Tepper, J., and Kornbrust, D. (2016). Considerations for the Characterization and Interpretation of Results Related to Alternative Complement Activation in Monkeys Associated with Oligonucleotide-Based Therapeutics. Nucleic Acid Therapeut. *26*, 210–215.
30. MacLellan, A., Nazal, B., Young, L., and Mason, G. (2022). Waking inactivity as a welfare indicator in laboratory mice: investigating postures, facial expressions and depression-like states. R. Soc. Open Sci. *9*, 221083.
31. Langford, D.J., Bailey, A.L., Chanda, M.L., Clarke, S.E., Drummond, T.E., Echols, S., Glick, S., Ingrao, J., Klassen-Ross, T., Lacroix-Fralish, M.L., et al. (2010). Coding of facial expressions of pain in the laboratory mouse. Nat. Methods *7*, 447–449.
32. Gaus, H.J., Gupta, R., Chappell, A.E., Østergaard, M.E., Swayze, E.E., and Seth, P.P. (2019). Characterization of the interactions of chemically-modified therapeutic nucleic acids with plasma proteins using a fluorescence polarization assay. Nucleic Acids Res. *47*, 1110–1122.
33. Crooke, S.T., Vickers, T.A., and Liang, X.H. (2020). Phosphorothioate modified oligonucleotide-protein interactions. Nucleic Acids Res. *48*, 5235–5253.

34. Iannitti, T., Morales-Medina, J.C., and Palmieri, B. (2014). Phosphorothioate oligonucleotides: effectiveness and toxicity. Curr. Drug Targets *15*, 663–673.

35. Østergaard, M.E., Jackson, M., Low, A., E Chappell, A., G Lee, R., Peralta, R.Q., Yu, J., Kinberger, G.A., Dan, A., Carty, R., et al. (2019). Conjugation of hydrophobic moieties enhances potency of antisense oligonucleotides in the muscle of rodents and non-human primates. Nucleic Acids Res. *47*, 6045–6058.

36. Wada, S., Yasuhara, H., Wada, F., Sawamura, M., Waki, R., Yamamoto, T., Harada-Shiba, M., and Obika, S. (2016). Evaluation of the effects of chemically different linkers on hepatic accumulations, cell tropism and gene silencing ability of cholesterol-conjugated antisense oligonucleotides. J. Contr. Release *226*, 57–65.

37. Blackmore, T.K., Sadlon, T.A., Ward, H.M., Lublin, D.M., and Gordon, D.L. (1996). Identification of a heparin binding domain in the seventh short consensus repeat of complement factor H. J. Immunol. *157*, 5422–5427.

38. Blackmore, T.K., Hellwage, J., Sadlon, T.A., Higgs, N., Zipfel, P.F., Ward, H.M., and Gordon, D.L. (1998). Identification of the second heparin-binding domain in human complement factor H. J. Immunol. *160*, 3342–3348.

39. Chi, X., Gatti, P., and Papoian, T. (2017). Safety of antisense oligonucleotide and siRNA-based therapeutics. Drug Discov. Today *22*, 823–833.

40. Sewing, S., Roth, A.B., Winter, M., Dieckmann, A., Bertinetti-Lapatki, C., Tessier, Y., McGinnis, C., Huber, S., Koller, E., Ploix, C., et al. (2017). Assessing single-stranded oligonucleotide drug-induced effects *in vitro* reveals key risk factors for thrombocytopenia. PLoS One *12*, e0187574.

41. Narayanan, P., Shen, L., Curtis, B.R., Bourdon, M.A., Nolan, J.P., Gupta, S., Hoffmaster, C., Zhou, F., Christian, B., Schaubhut, J.L., et al. (2018). Investigation into the Mechanism(s) That Leads to Platelet Decreases in Cynomolgus Monkeys During Administration of ISIS 104838, a 2'-MOE-Modified Antisense Oligonucleotide. Toxicol. Sci. *164*, 613–626.

42. Slingsby, M.H.L., Vijey, P., Tsai, I.T., Roweth, H., Couldwell, G., Wilkie, A.R., Gaus, H., Goolsby, J.M., Okazaki, R., Terkovich, B.E., et al. (2022). Sequence-specific 2'-O-methoxyethyl antisense oligonucleotides activate human platelets through glycoprotein VI, triggering formation of platelet-leukocyte aggregates. Haematologica *107*, 519–531.

43. Jaax, M.E., Krauel, K., Marschall, T., Brandt, S., Gansler, J., Fürll, B., Appel, B., Fischer, S., Block, S., Helm, C.A., et al. (2013). Complex formation with nucleic acids and aptamers alters the antigenic properties of platelet factor 4. Blood *122*, 272–281.

44. van Meer, L., Moerland, M., Gallagher, J., van Doorn, M.B.A., Prens, E.P., Cohen, A.F., Rissmann, R., and Burggraaf, J. (2016). Injection site reactions after subcutaneous oligonucleotide therapy. Br. J. Clin. Pharmacol. *82*, 340–351.

45. Turner, P.V., Pekow, C., Vasbinder, M.A., and Brabb, T. (2011). Administration of substances to laboratory animals: equipment considerations, vehicle selection, and solute preparation. J. Am. Assoc. Lab. Anim. Sci. *50*, 614–627.

46. Migawa, M.T., Shen, W., Wan, W.B., Vasquez, G., Oestergaard, M.E., Low, A., De Hoyos, C.L., Gupta, R., Murray, S., Tanowitz, M., et al. (2019). Site-specific replacement of phosphorothioate with alkyl phosphonate linkages enhances the therapeutic profile of gapmer ASOs by modulating interactions with cellular proteins. Nucleic Acids Res. *47*, 5465–5479.

47. Shen, W., De Hoyos, C.L., Migawa, M.T., Vickers, T.A., Sun, H., Low, A., Bell, T.A., III, Rahdar, M., Mukhopadhyay, S., Hart, C.E., et al. (2019). Chemical modification of PS-ASO therapeutics reduces cellular protein-binding and improves the therapeutic index. Nat. Biotechnol. *37*, 640–650.

48. Anderson, B.A., Freestone, G.C., Low, A., De-Hoyos, C.L., Iii, W.J.D., Østergaard, M.E., Migawa, M.T., Fazio, M., Wan, W.B., Berdeja, A., et al. (2021). Towards next generation antisense oligonucleotides: mesylphosphoramidate modification improves therapeutic index and duration of effect of gapmer antisense oligonucleotides. Nucleic Acids Res. *49*, 9026–9041.

49. Kim, B., Park, J.H., and Sailor, M.J. (2019). Rekindling RNAi Therapy: Materials Design Requirements for In Vivo siRNA Delivery. Adv. Mater. *31*, e1903637.

50. Buck, J., Grossen, P., Cullis, P.R., Huwyler, J., and Witzigmann, D. (2019). Lipid-Based DNA Therapeutics: Hallmarks of Non-Viral Gene Delivery. ACS Nano *13*, 3754–3782.